Check for updates

View Article Online
View Journal

Nanoscale

Accepted Manuscript

This article can be cited before page numbers have been issued, to do this please use: H. Song, C. Ma, L. Wang and Z. Zhu, *Nanoscale*, 2020, DOI: 10.1039/D0NR04060F.

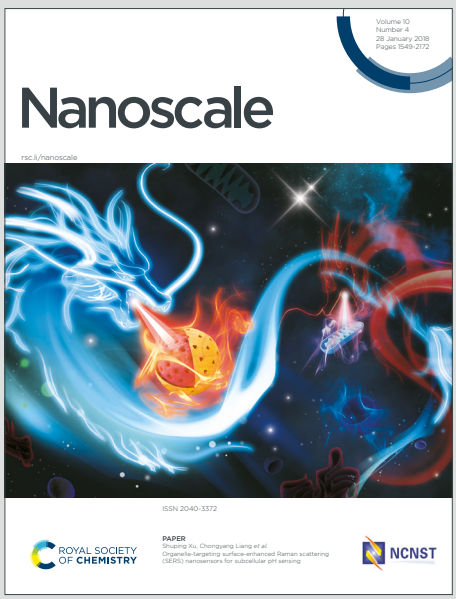

This is an Accepted Manuscript, which has been through the Royal Society of Chemistry peer review process and has been accepted for publication.

Accepted Manuscripts are published online shortly after acceptance, before technical editing, formatting and proof reading. Using this free service, authors can make their results available to the community, in citable form, before we publish the edited article. We will replace this Accepted Manuscript with the edited and formatted Advance Article as soon as it is available.

You can find more information about Accepted Manuscripts in the Information for Authors.

Please note that technical editing may introduce minor changes to the text and/or graphics, which may alter content. The journal's standard Terms & Conditions and the Ethical guidelines still apply. In no event shall the Royal Society of Chemistry be held responsible for any errors or omissions in this Accepted Manuscript or any consequences arising from the use of any information it contains.

ROYAL SOCIETY OF CHEMISTRY

rsc.li/nanoscale

View Article Online
DOI: 10.1039/D0NR04060F

Platinum Nanoparticles-Deposited Multiwalled Carbon Nanotubes as a NADH Oxidase Mimic: Characterization and Application

Haiyan Song,[a] Chunling Ma,[a] Lei Wang,[c] Zhiguang Zhu[a,b,*]

[a] Tianjin Institute of Industrial Biotechnology, Chinese Academy of Sciences, 32 West Seventh Avenue, Tianjin Airport Economic Area, Tianjin, 300308, P. R. China

[b] School of Chemical Engineering, University of Chinese Academy of Sciences, 19A Yuquan Road, Shijingshan District, Beijing, 100049, P. R. China

[c] National Human Genetic Resource Center, 12 Dahuisi Road, Haidian District, Beijing 100081, P.R. China

[*]Corresponding Author: Zhiguang Zhu (zhu_zg@tib.cas.cn), ORCID: 0000-0002-6625-5087

Tel: (+86)-022-2482 8797; Fax: (+86)-022-8486 1926

Published on 21 August 2020. Downloaded by University of Rochester on 8/25/2020 9:36:17 PM.

Nanoscale Accepted Manuscript

View Article Online
DOI: 10.1039/D0NR04060F

Published on 21 August 2020. Downloaded by University of Rochester on 8/25/2020 9:36:17 PM.

Nanoscale Accepted Manuscript

Abstract

The effective regeneration of bioactive NAD^+ plays an important role in numerous dehydrogenase-dependent applications including biocatalysis and biosensing. However, this process usually suffers from high thermodynamic barrier, instability and high cost associated with natural enzymes. The emergence of nanomaterials with enzyme mimic characteristics has offered a potent alternative to many enzyme-catalyzed processes. Platinum nanoparticles (PtNPs), for example, have been extensively studied for their peroxidase and oxidase-like activities. However, their behavior as a NADH oxidase mimic has barely been characterized in detail. Herein, we report a facile approach to prepare PtNPs-deposited multiwalled carbon nanotubes (PtNPs@MWCNTs) as the nanozyme for NADH oxidation. Its enzymatic activity was in-depth investigated, revealing that it was a NADH oxidase instead of a peroxidase and the catalytic process generated $O_2^{-\bullet}$, rather than $OH^\bullet$ or $^1O_2$, from dissolved O_2. The recovery yield of bioactive NAD^+ regeneration by the nanozyme could reach ~100% with a total turnover number of ~6000. Besides, it exhibited terrific electrochemical performance for NADH oxidation and sensing by greatly boosting the response and lowering the oxidation overpotential. Moreover, it could also work on biomimetic cofactors with even higher activity. Finally, xylose dehydrogenase was immobilized with the nanozyme to constitute a hybrid bioelectrode for xylose sesning. The biosensor had a xylose detecting range of 5-400 μM with the limit of detection as low as 1 μM and can retain its performance after being reused for several times. Our results suggest that the PtNPs@MWCNTs characterized as a NADH oxidase nanozyme hold great promise in the applications of biocatalysis and biosensing, which intensively deal with dehydrogenases and natural or biomimetic cofactors.

Keywords: nanozyme; NADH oxidase; PtNPs@MWCNTs; NAD^+ regeneration; biomimetic cofactor; biosensor

View Article Online
DOI: 10.1039/D0NR04060F

Published on 21 August 2020. Downloaded by University of Rochester on 8/25/2020 9:36:17 PM.

Introduction

The intrinsic limitations of natural enzymes, such as prone to denaturation under unfavorable conditions, high cost and time-consuming preparation associated with purification processes, have driven the development of nanomaterials as alternatives. Among them, some so-called nanozymes not only exhibit outstanding enzyme-like catalytic performance and good selectivity, but also feature high operational and storage stability as well as facile preparation, thus being regarded as the next generation enzyme mimics.[1-6] Since the pioneering work of discovering Fe_3O_4 nanoparticles as a peroxidase mimic by Yan et al. on 2007,[7] a plethora of inorganic nanomaterials have been investigated for enzyme-mimicking properties, including metal nanoparticles, nanoclusters, or nanorods, metal oxides, single-atom metals, and so on.[8-11] More recently, nanocomposites comprised of a catalytic core and a capping or supporting layer have been widely adopted to construct a nanozyme, as the activity, stability, and the dispersibility of the catalytic core can be regulated or improved by the capping or supporting layer.[12-16] In terms of enzyme category, peroxidase and oxidase mimics are the most studied, while mimics of catalase, superoxide dismutase, hydrolase and others are also frequently reported.[1] Over the last decade, the exploration of nanozymes, along with the advances in nanotechnology and biotechnology, bring the opportunity to leverage and expand the realm of enzymatic catalysis by elucidating catalytic mechanisms, designing facilitated reaction routes, and demonstrating versatile applications. Numerous examples of *in vitro* sensing of H_2O_2, glucose, lactate, xanthine, dopamine, and Cr (VI) ions, *in vivo* sensing, imaging, and therapeutics with the use of nanozymes have been presented, suggesting their enormous potential.[12, 17-24]

Nicotinamide adenine dinucleotide (NAD^+) and its reduced form (NADH) are essential cofactors in nature and play important roles in cell metabolism and biological electron transfer reactions. The bioactive NAD^+ regeneration is of tremendous value to reactions mediated by most dehydrogenases in the applications of biosensors, biofuel cells, and biocatalysis.[25-27] Especially in electrochemical biosensors relying on dehydrogenases, the typical bioactive NAD^+ regeneration at

Nanoscale Accepted Manuscript

View Article Online
DOI: 10.1039/D0NR04060F

Published on 21 August 2020. Downloaded by University of Rochester on 8/25/2020 9:36:17 PM.

conventional solid electrodes requires considerable activation energy (i.e., high overpotential) and often couples with undesired side reactions and irreversibility with the formation of inactive dimers. To overcome these challenges, various nanomaterials have been actively exploited for electrochemical sensing and oxidation of NADH, for instance, inorganic materials including Au, Pt, Cu, Pd, or bimetallic ones and carbon based materials such as treated multiwalled carbon nanotubes (MWCNTs), nitrogen-doped graphene, and carbon nitride.[28-32] Platinum nanoparticles (PtNPs), particularly, have been explored to mimic various peroxidases and oxidases with excellent catalytic performance.[8, 13, 33, 34] For example, PtNPs@MnO_2 was reported to display a typical Michaelis-Menten behavior as a general oxidase rather than a peroxidase and was applied in colorimetric assays for detecting glutathione and dopamine.[13] Albert with enhanced catalytic efficiency and turnover achieved as shown in numerous literatures, PtNPs have barely been characterized in detail for their NADH oxidase-like activity yet. In addition, the common approach to perform NADH electrooxidation at a low overpotential is historically represented by the use of redox mediators along with the nanomaterials.[27, 35, 36] Although the rationale for the selection of the proper mediators and their possible kinetic and thermodynamic constraints could be addressed, the mediator-free approach is more favorable.

In this study, we constructed a PtNPs-deposited MWCNTs nanocomposite (PtNPs@MWCNTs) and investigated its nanozyme behavior in detail for NADH oxidation. MWCNTs was chosen since they have been steadily developed and frequently applied in sensors,[37] supercapacitors,[38] and fuel cells[39] due to their large specific surface area and excellent biocompatibility as carriers, good electrocatalytic property as catalysts and superior conductivity as electronic wires.[40] They could be used as a model nanomaterial and provide a conductive and stable support for PtNPs, allowing the good activity and stability of the catalytic core. The possible reaction mechanism was exploited by determining the product and identifying the possible intermediate reactive oxygen species (ROS). Besides on the natural NADH, the activity of PtNPs@MWCNTs on the biomimetic cofactor (e.g. N-benzyl nicotinamide (BNAH)) was also evaluated. The application of this NADH oxidase-mimic was

Nanoscale Accepted Manuscript

View Article Online
DOI: 10.1039/D0NR04060F

further demonstrated on a mediator-free xylose-sensing bioelectrode assembled, with high sensitivity and good stability achieved. These results suggest that the PtNPs@MWCNTs characterized as a NADH oxidase nanozyme hold great promise in biocatalytic reactions and pave the way for the construction of dehydrogenase-based biosensors relying on natural or biomimetic cofactors.

Published on 21 August 2020. Downloaded by University of Rochester on 8/25/2020 9:36:17 PM.

Results and discussion

Morphology of the PtNPs@MWCNTs

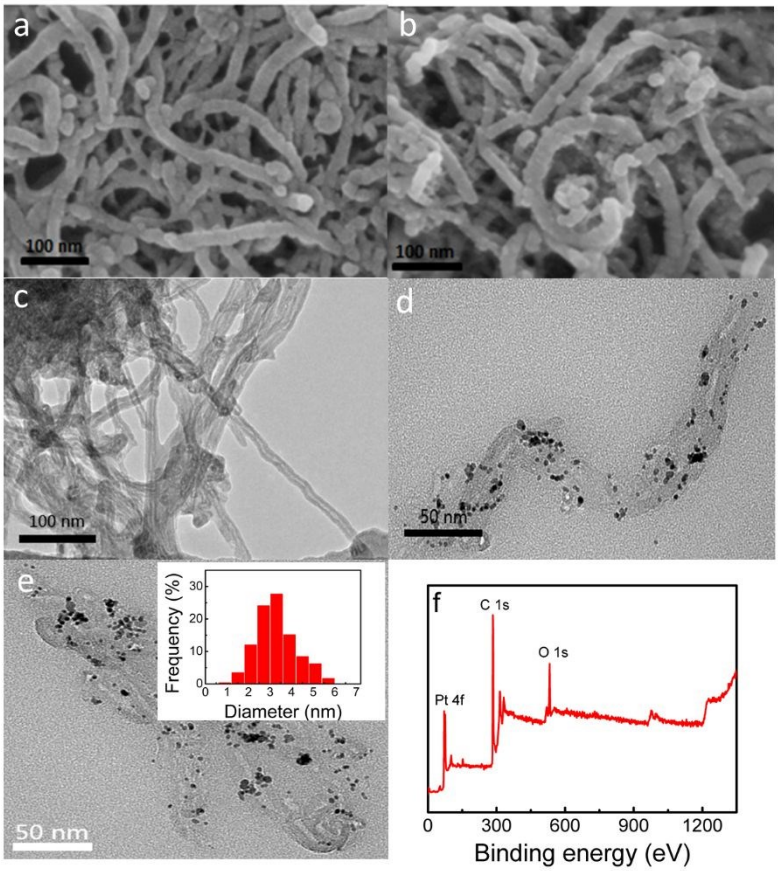

Fig. 1. SEM images of (a) MWCNTs and (b) PtNPs@MWCNTs, TEM of (c) MWCNTs and (d) PtNPs@MWCNTs, (e) Average diameter of PtNPs, and (f) XPS of PtNPs@MWCNTs.

The morphology of the PtNPs@MWCNTs was characterized by SEM and TEM. As displayed in Fig. 1a and 1c, MWCNTs present an ideal tubular structure with a relatively smooth surface and the surface area of ~101.4±0.4 $m^2 g^{-1}$ measured by BET.

Nanoscale Accepted Manuscript

View Article Online
DOI: 10.1039/D0NR04060F

The solid PtNPs are distributed on the outer surface of MWCNTs (Fig. 1b and 1d), with an average particle diameter of ~3.3 nm (Fig. 1e), in agreement with those reported in literature[41, 42]. Moreover, a qualitative analysis of the surface composition of the PtNPs@MWCNTs was surveyed by XPS and the successful attachment of PtNPs on the surface of MWCNTs could be confirmed (Fig. 1f).

Published on 21 August 2020. Downloaded by University of Rochester on 8/25/2020 9:36:17 PM.

Catalytic activity and mechanism of the PtNPs@MWCNTs

The oxidase-like catalytic activity of the PtNPs@MWCNTs for NADH was intensively evaluated. As shown in Fig. 2a, the absorbance at 340 nm of the NADH solution reduces with the reaction time in presence of the PtNPs@MWCNTs, validating the oxidase-like catalytic activity of the PtNPs@MWCNTs. With the same loading of the MWCNTs, the absorbance at 340 nm decreases slightly, similar to that of the sample with NADH alone or PtNPs@MWCNTs alone, suggesting that the introduction of MWCNTs has a negligible effect on NADH oxidation. Then, we explored the catalytic mechanism of PtNPs@MWCNTs nanozyme. In Fig. 2b, the NADH solution bubbled with N_2 can barely be oxidized by the PtNPs@MWCNTs. Conversely, when bubbled with O_2 or air, the NADH amount decreases dramatically, revealing that O_2 plays a key role in the catalysis mediated by the PtNPs@MWCNTs nanozyme.

Furthermore, inspired from the natural NADH oxidase, which could produce H_2O_2 or H_2O during the NADH oxidation resulted from two different catalytic mechanisms, we investigated whether H_2O_2 was produced in the NADH oxidation with the use of PtNPs@MWCNTs nanozyme. A typical peroxidase substrate TMB was chosen as the chromogenic substrate and it would be oxidized by H_2O_2 under the catalysis of HRP. The result shows that the nanozyme exhibits a weak catalytic activity towards TMB in the presence of dissolved O_2, even without HRP (Fig. S1a). Next, we run the NADH oxidation reaction mediated by the nanozyme for a while and stopped the reaction by spinning out the nanozyme. The as-obtained solution was then bubbled with N_2 and added with TMB and HRP, however, yielding no absorbance increase at 650 nm. When further added with H_2O_2, the solution displays a distinct absorbance increase,

Nanoscale Accepted Manuscript

View Article Online
DOI: 10.1039/D0NR04060F

proving that H_2O_2 is not the reaction product of NADH oxidation mediated by the PtNPs@MWCNTs nanozyme (Fig. S1b).

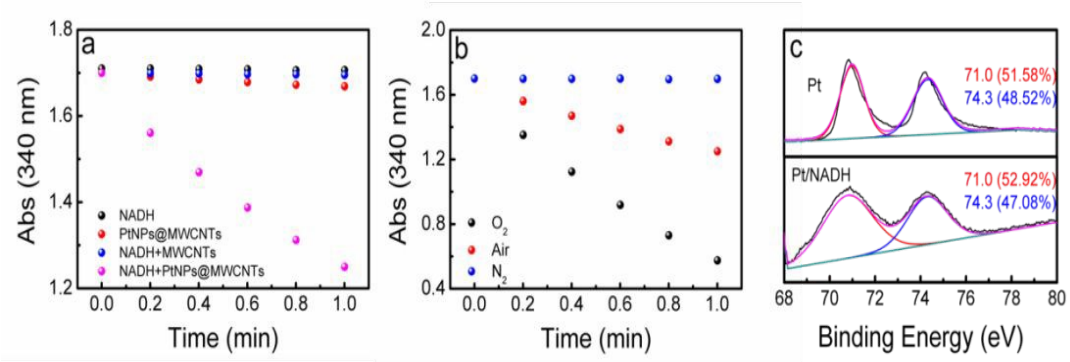

Fig. 2. Time-dependent absorbance changes at 340 nm for NADH. (a) Catalytic activity of PtNPs@MWCNTs for NADH oxidation, (b) Influences of O_2, air or N_2 on the NADH oxidation, (c) High-resolution XPS Pt 4f spectrum of PtNPs@MWCNTs. NADH: 0.2 mM, PtNPs@MWCNTs: 0.4 mg mL^{-1}, MWCNTs: 0.4 mg mL^{-1}.

Moreover, according to the catalytic mechanism of other nanozymes reported, which was always associated with the generation of intermediate ROS,[43, 44] we investigated the NADH oxidation mediated by the PtNPs@MWCNTs nanozyme in the presence of two radical scavengers to identify the possible ROS produced in our case. As a result, the NADH oxidation is largely unaffected in presence of different concentrations of NaN_3, a well-known $OH^{\bullet}$ and $^1O_2$ scavenger (Fig. S2a).[45] However, the NADH oxidation decreases significantly with the increase of the concentration of SOD, a well-known $O_2^{-\bullet}$ scavenger (Fig. S2b),[45] suggesting that $O_2^{-\bullet}$ may be excited as a underlying factor for the NADH oxidation mediated by the nanozyme.

Furthermore, the surface states of PtNPs before and after the catalytic oxidation of NADH were monitored using XPS. Based on Fig. 2c, the spectra of Pt 4f peaks reveal little variation in Pt^0 (71.0 eV) and Pt^{2+} (74.3 eV) contents before and after the catalysis, essentially indicating that Pt^0 and Pt^{2+} can be effectively recycled. Thereby, the above-mentioned results substantially demonstrate that PtNPs attached on MWCNTs serve as a NADH oxidase mimic. A possible mechanism for the

Published on 21 August 2020. Downloaded by University of Rochester on 8/25/2020 9:36:17 PM.

Nanoscale Accepted Manuscript

View Article Online
DOI: 10.1039/D0NR04060F

oxidase-like activity of PtNPs@MWCNTs nanozyme was speculated as follows:

$$2O_2 \xrightarrow{PtNPs@MWCNTs} 2O_2^{-\cdot}$$

$$2O_2^{-\cdot} + 3NADH + 5H^+ \rightarrow 3NAD^+ + 4H_2O$$

Enzymatic properties of the PtNPs@MWCNTs

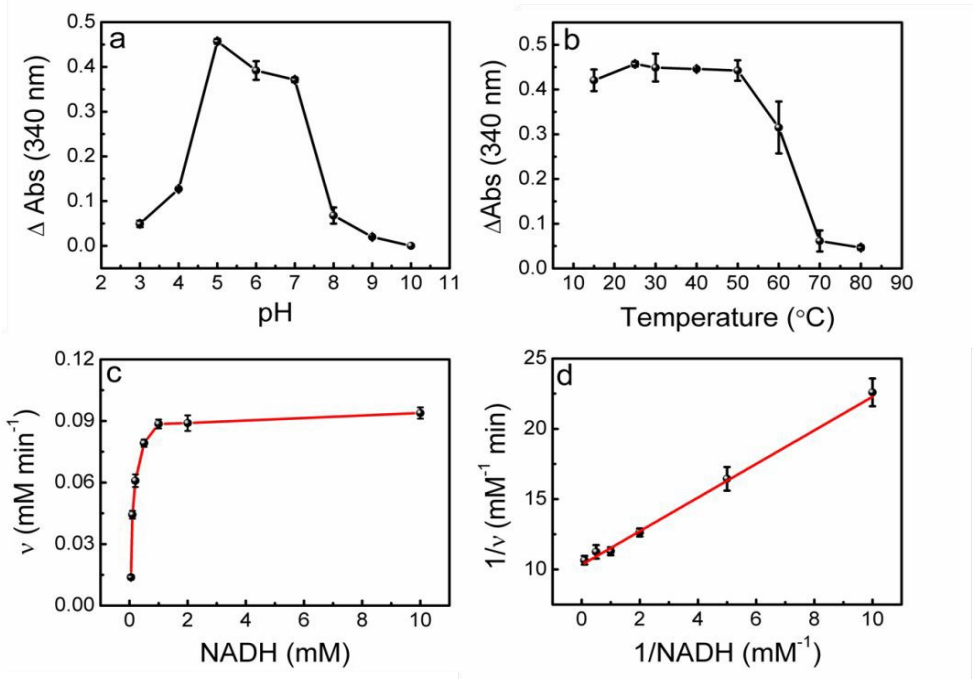

Fig. 3. Catalytic activity of PtNPs@MWCNTs for NADH at (a) different pHs of 3.0-10.0 and (b) temperatures of 15-80 °C, (c) Steady-state kinetic assay of PtNPs@MWCNTs for NADH, (d) Double reciprocal plot of the nanozyme activity.

To explore the enzymatic properties of PtNPs@MWCNTs, the NADH oxidation reaction was firstly optimized at different pH values (3.0-10.0) and temperatures (15-80 °C). Notably, the PtNPs@MWCNTs exhibits the maximum catalytic activity at pH 5.0, consistent with several other Pt-based nanozymes (Fig. 3a).[46] The nanozyme retains a high catalytic activity over the temperature range of 15-50 °C, with the observed activity rapidly decreasing at higher temperatures (Fig. 3b), possibly due to the instability of the reaction product at elevated temperatures.[47] Moreover, we obtained the Michaelis-Menten constant of the nanozyme. K_m, representing the substrate affinity to the enzyme, was determined as 0.14 mM and the

Published on 21 August 2020. Downloaded by University of Rochester on 8/25/2020 9:36:17 PM.

Nanoscale Accepted Manuscript

View Article Online
DOI: 10.1039/D0NR04060F

K_{cat}, representing the turnover rate of the nanozyme, was 0.021 s^{-1} (Fig. 3c and 3d). Although the K_{cat} is slightly lower than that of several natural NADH oxidases, which may be ascribed to the poor loading of PtNPs onto the MWCNTs, it is enough to accomplish the bioactive NAD^+ regeneration and presents much better stability than that of natural NADH oxidases. Additionally, we found that there was a good linear relationship between the absorbance change and the NADH concentration ranging from 1 to 200 μM with a limit of detection (LOD) of 0.8 μM (Fig. S3).

Bioactive NAD^+ regeneration by the PtNPs@MWCNTs

To demonstrate the ability of the PtNPs@MWCNTs nanozyme for biotechnological applications, it is essential to prove the conversion of NADH into bioactive NAD^+ and proceed a biocatalytic reaction driven by the cofactor regeneration. To achieve this goal, the PtNPs@MWCNTs nanozyme system was coupled to the FDH-catalyzed oxidation of formate, which involved with the reduction of bioactive NAD^+. First, 0.2 mM NADH was almost fully oxidized by the PtNPs@MWCNTs nanozyme, as depicted in the blue curve of Fig. 4a. After the nanozyme was removed by centrifugation and fresh FDH and formate were subsequently added, 0.2 mM NADH could be obtained with a recovery yield of ~100 % (red curve, Fig. 4a), illustrating that PtNPs@MWCNTs nanozyme can efficiently regenerate bioactive NAD^+. In addition, we investigated that total turnover number (TTN) of the nanozyme in an enzyme-nanozyme hybrid catalytic system containing 5 M formate, 10 U FDH, 0.5 mM NAD^+ and 0.4 mg mL^{-1} nanozyme. It was found that the formate concentration decreased to ~2 M after 32 h and the TTN was calculated as ~6000, demonstrating the great application potential of the nanozyme.[48, 49]

Published on 21 August 2020. Downloaded by University of Rochester on 8/25/2020 9:36:17 PM.

Nanoscale Accepted Manuscript

View Article Online
DOI: 10.1039/D0NR04060F

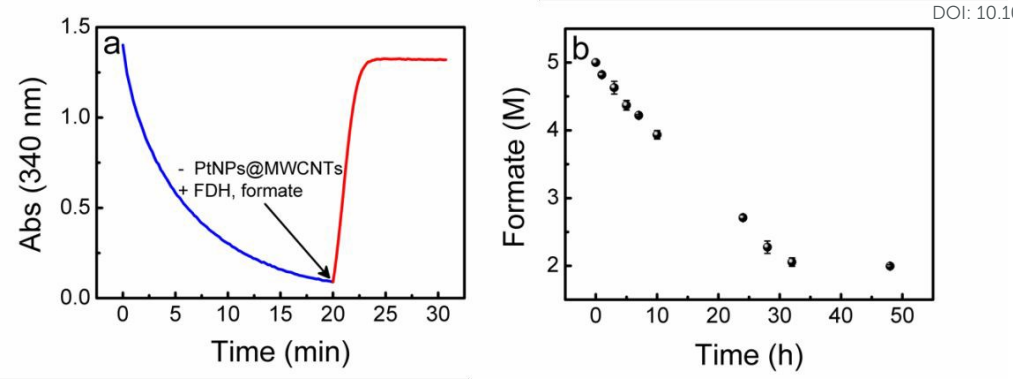

Fig. 4. (a) UV-vis absorption-time course curve for NADH at 340 nm. Blue: 0.2 mM NADH and 0.4 mg mL^{-1} PtNPs@MWCNTs, Red: remove the nanozyme and add 10 U FDH and 50 mM formate, (b) The consumption of the formate in the enzyme-nanozyme hybrid catalytic system.

Electrochemical performance of the PtNPs@MWCNTs

Next, we investigated the electrocatalytic activity of the PtNPs@MWCNTs nanozyme in detail. From the CV result, an obvious anodic peak current appears when using a bare glassy carbon electrode (GCE), MWCNTs-decorated GCE or PtNPs@MWCNTs-decorated GCE in 0.1 M PBS containing NADH (Fig. S4). Notably, MWCNTs deposited at the GCE could reduce the overpotential of NADH oxidation, shifting the E_p value negatively by 400 mV to 0.1 V vs Ag/AgCl (Fig. 5a)[50], and enhance the oxidation current nearly by 5 times. The deposition of PtNPs onto MWCNTs can barely further reduce the oxidation overpotential of NADH, but significantly enhance the peak current by nearly 50 % (Fig. 5a), largely due to the excellent conductivity of the PtNPs. This result can also be found when comparing Fig. S4b and S4c. Additionally, the oxidation peak current at ~0.1 V increases with the NADH concentration rising from 0 to 4 mM (Fig. 5b). This oxidation peak current greatly increases when bubbled by N_2 and decreases when bubbled by O_2 (Fig. 5c), illustrating that the O_2 involved in the enzymatic oxidation of NADH by the nanozyme would compete with the anodic electrooxidation of NADH. In brief, the nanozyme exhibits terrific electrochemical performance for NADH oxidation and sensing, by amplifying the response greatly and lowering the oxidation overpotential.

Published on 21 August 2020. Downloaded by University of Rochester on 8/25/2020 9:36:17 PM.

Nanoscale Accepted Manuscript

View Article Online
DOI: 10.1039/D0NR04060F

Published on 21 August 2020. Downloaded by University of Rochester on 8/25/2020 9:36:17 PM.

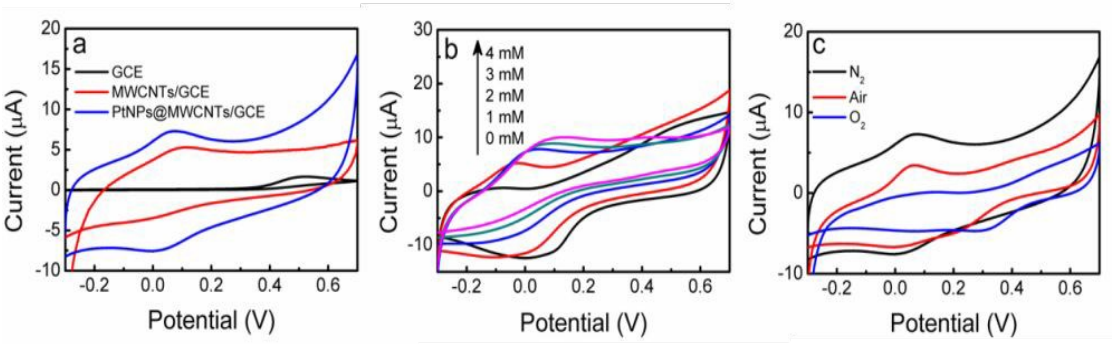

Fig. 5. (a) CVs of GCE, MWCNTs/GCE and PtNPs@MWCNTs/GCE in 0.1 M PBS containing 1 mM NADH, (b) CVs at PtNPs@MWCNTs/GCE with various NADH concentrations, (c) CVs of PtNPs@MWCNTs/GCE with N_2, air or O_2. Scan rate: 10 mV s^{-1}.

Evaluation of the PtNPs@MWCNTs for biomimetic cofactors

Although widely used, the natural cofactors such as NADH are prohibitively expensive and chemically unstable.[51] These drawbacks have driven the seek of more stable synthetic nicotinamide cofactor analogues that can interface with enzyme catalysts.[52-54] Recently, BNAH, nicotinamide riboside (NRH), and nicotinamide mononucleotide (NMNH) as alternatives of NADH have been applied in biotransformation and bioelectricity generation with the successful development of corresponding engineered enzymes (Fig. S5).[55-57] Herein, we chose BNAH as an example and investigated the catalytic activity of the PtNPs@MWCNTs nanozyme on this biomimetic cofactor. Similar to NADH, PtNPs deposited onto MWCNTs present a significant BNAH oxidation activity (Fig. 6a). K_m and K_{cat} are 0.452 mM and 0.066 s^{-1}, even better than those for NADH (Fig. 6b and 6c). The oxidation peak potential occurs at -0.1 V and the oxidation peak current increases as a function of various BNAH concentrations (Fig. 6d). All these results indicate that the PtNPs@MWCNTs nanozyme demonstrates great potential in oxidizing biomimetic cofactors and could be used in a diverse of biomimicking catalytic systems in the future.

Nanoscale Accepted Manuscript

View Article Online
DOI: 10.1039/D0NR04060F

Published on 21 August 2020. Downloaded by University of Rochester on 8/25/2020 9:36:17 PM.

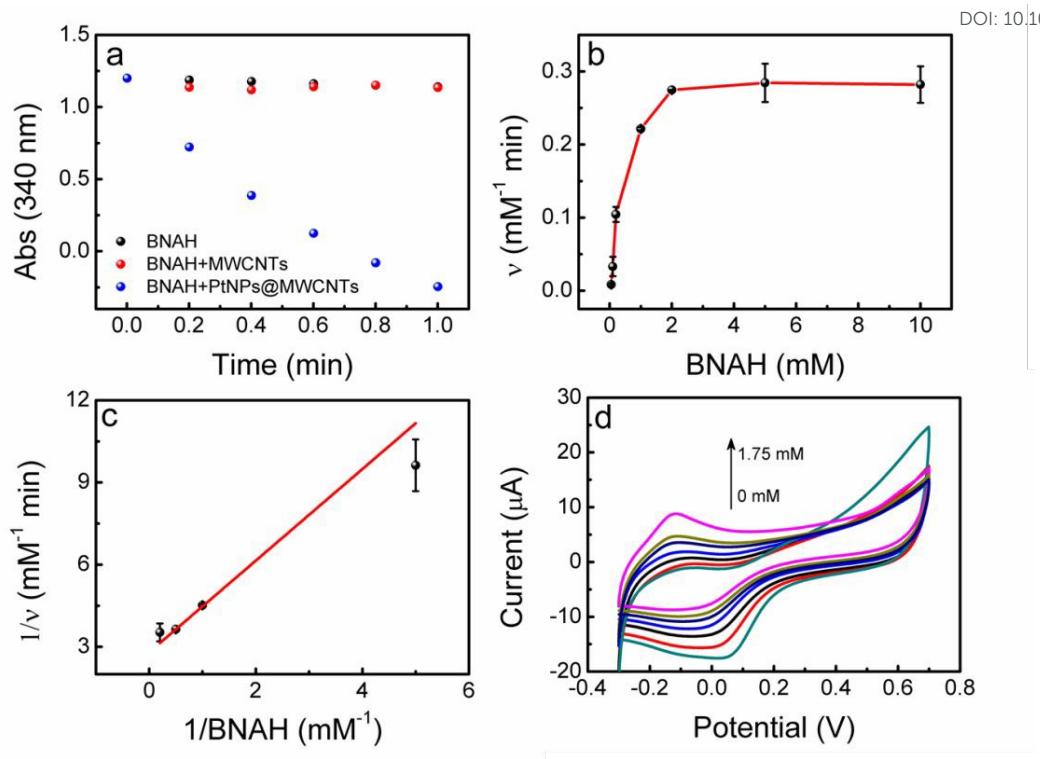

Fig. 6. (a) Time-dependent absorbance changes at 340 nm for BNAH. BNAH: 0.5 mM, MWCNTs: 0.2 mg mL^{-1}, PtNPs@MWCNTs: 0.2 mg mL^{-1}, (b) Steady-state kinetic assay of PtNPs@MWCNTs for BNAH, (c) Double reciprocal plot of the nanozyme activity for BNAH, (d) CVs at PtNPs@MWCNTs/GCE in 0.1 M PBS containing 0, 0.05, 0.3, 0.75, 1.00, 1.25, or 1.75 mM BNAH.

Application of the PtNPs@MWCNTs in a xylose biosensor

More than 300 kinds of dehydrogenases in nature depend on NADH as an electron transporter. However, the electrochemical biosensors based on natural dehydrogenases always suffer from poor regeneration of bioactive NAD^+, stability issues with enzymes and cofactors, and use of toxic and expensive electron mediators. Herein, we took XDH as an example and aimed to construct a mediator-free xylose biosensor, in which NAD^+ was reduced during the xylose oxidation by XDH and then electrochemically regenerated by the nanozyme. The XDH was obtained from *C. vibrioides* and was well expressed in *E. coli* (Fig. S6a), exhibiting the enzymatic activity of ~8 U mg^{-1}.[58] XDH was then successfully immobilized on PtNPs@MWCNTs via the amide bond, as indicated from Fig. S6b showing two broad

Nanoscale Accepted Manuscript

View Article Online
DOI: 10.1039/D0NR04060F

characteristic bands at 1640 and 1554 cm^{-1}, commonly labelled as amide I and amide II.[59] Additionally, EIS was performed to probe the features of the surface-modified electrode. Fig. S6c shows a Nyquist plot of different electrodes in 5 mM $K_3Fe(CN)_6/K_4Fe(CN)_6$ redox probe in 0.1 M KCl. The bare GCE displays a small resistance, while the resistance of the PtNPs@MWCNTs electrode is even smaller, illustrating the excellent electrically conductivity of PtNPs@MWCNTs. Upon the immobilization of XDH, an insulating protein layer was formed at the electrode surface, evident from the appearance of a significantly increased semicircular portion of the resulting spectrum. These results further indicate the successful XDH immobilization. Moreover, the bioelectrode preparation was optimized. Fig. S7a reveals that the immobilized XDH amount increases with the applied XDH amount and the current response also increases with immobilized XDH amount until reaching 100 mU. Fig. S7b shows that the optimal pH of the bioelectrode is 7.0.

Finally, the prepared bioelectrode was investigated for xylose detection. As shown in Fig. 7a, the oxidation peak current appears at ~0.25 V as a result of NADH electrochemical oxidation and increases with the increase of xylose concentration. The oxidation overpotential shifts towards the positive potential by 150 mV compared to that of the PtNPs@MWCNTs/GCE, possibly caused by the immobilization of insulating XDH. A well-defined linear relationship between the current response and xylose concentration can be observed from 5 to 400 μM (Fig. 7b). The regression equation is $\Delta i_p=17.63\lg c_{xylose}-8.42$ with a correlation coefficient of 0.999. The LOD of 1 μM can be estimated at a signal-to-noise (S/N) ratio of 3. Additionally, we investigated the substrate selectivity of the biosensor constructed. The current response to the addition of 0.5 mM xylose or a series of other saccharides including maltose, mannose, glucose, fructose, sucrose, ribose, arabinose, galactose (100 mM respectively) was recorded. In contrast to xylose, other saccharides barely exhibited any current response, suggesting the good selectivity of the biosensor (Fig. 7c). More gratifyingly, the current response of XDH&PtNPs@MWCNTs/GCE remains 95% of its initial value after successive additions of 1 mM xylose for 5 times (Fig. 7d). In contrast, the current response of XDH@MWCNTs/GCE gradually decreases. The

Published on 21 August 2020. Downloaded by University of Rochester on 8/25/2020 9:36:17 PM.

Nanoscale Accepted Manuscript

View Article Online
DOI: 10.1039/D0NR04060F

Published on 21 August 2020. Downloaded by University of Rochester on 8/25/2020 9:36:17 PM.

Nanoscale Accepted Manuscript

performance of the biosensor still remains 81.2% of its initial performance after 5 days, demonstrating its favorable stability (Fig. 7e). This result again suggests that the use of the PtNPs@MWCNTs enables the effective regeneration of bioactive NAD^+ and greatly enhances the stability of the biosensor. Further, we evaluated the performance of the biosensor by measuring the xylose content in real samples (Fig. 7f). Apparently, the results of the xylose content in pretreated corncob measured by the biosensor and HPLC are in good agreement, illustrating that the biosensor based on the PtNPs@MWCNTs nanozyme is capable of precisely quantifying the xylose content in real lignocellulosic samples.

Compared with other NADH oxidase mimic based biosensors, the use of PtNPs@MWCNTs nanozyme, featuring efficient bioactive NAD^+ regeneration and facile preparation, exhibits obvious advantages. For example, in a MnO_2-TMB-based sensing platform for monitoring NAD^+-dependent reactions, the NADH generated triggers the decomposition of MnO_2 nanosheets and results in the slow down of color development and a gradually decreasing signal. This method, therefore, suffers from limited detection range and limit.[60] In another example, the use of hemin/G-quadruplex as a NADH oxidase mimic requires H_2O_2 as a co-reagent, thus making the operation too complicated.[61]

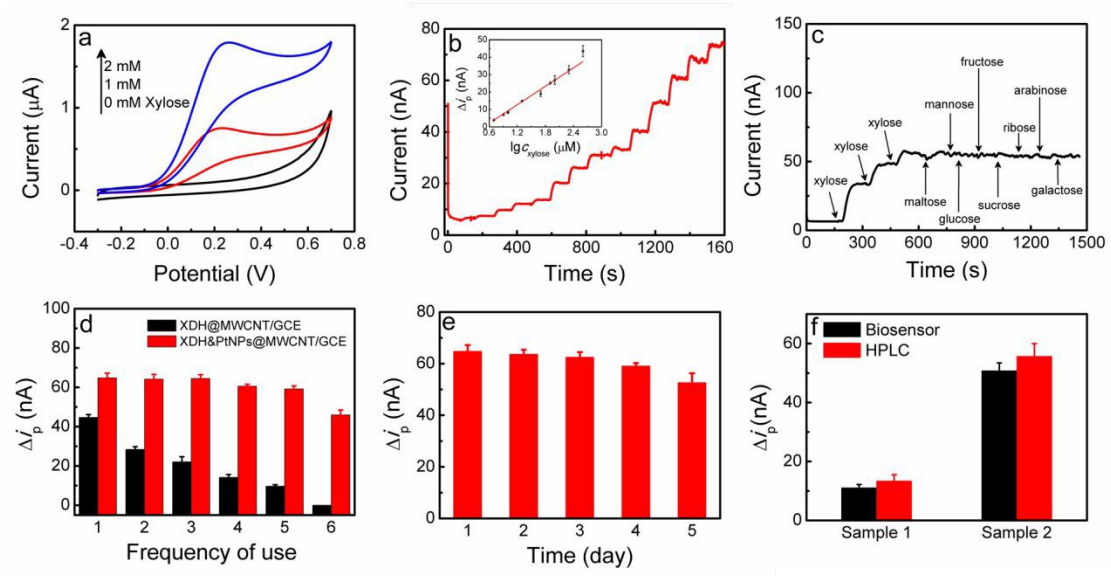

Fig. 7. (a) CVs of XDH&PtNPs@MWCNTs/GCE in 0.1 M PBS (pH 7.0) containing

View Article Online
DOI: 10.1039/D0NR04060F

1 mM NAD^+ and 0-2 mM xylose, (b) Typical calibration plot for xylose sensing using XDH&PtNPs@MWCNTs/GCE in 0.1 M PBS with various concentrations of xylose (Inset: amperometric time curve with the stepwise addition of xylose at 0.25 V), (c) Substrate specificity of the xylose biosensor, (d) Frequency of use of XDH@MWCNTs/GCE and XDH&PtNPs@MWCNTs/GCE in 0.1 M PBS (pH 7.0) containing 1 mM NAD^+ with the stepwise addition of 1 mM xylose, (e) Stability of the biosensor, (f) Analysis of real samples.

Published on 21 August 2020. Downloaded by University of Rochester on 8/25/2020 9:36:17 PM.

Conclusions

In summary, we prepared the PtNPs@MWCNTs nanocomposite using one-step chemical synthesis. The PtNPs@MWCNTs allowed for the bioactive NAD^+ regeneration using $O_2^{-\bullet}$, generated from dissolved O_2, which was defined to mimic the activity of NADH oxidase. The PtNPs@MWCNTs nanozyme coupled with the FDH confirmed that the nanozyme can be applied in the cofactor-dependent biocatalysis. Moreover, the nanozyme exhibited a superior activity for the biomimetic cofactor, paving the way for more applications in biomimicking catalysis in the future. In addition, PtNPs@MWCNTs nanozyme was also used for electrochemical biosensors based on a dehydrogenase, yielding a great sensitivity, selectivity, and stability. Future efforts should be focused on the optimization of the PtNPs@MWCNTs and the increase of its catalytic performance. More novel supporting nanomaterials for the PtNPs catalytic core can be tested as well in order to tune the nanozyme performance.

Nanoscale Accepted Manuscript

Experimental

Materials

Ethylene glycol, NAD^+, NADH, glucose, maltose, mannose, fructose, sucrose, ribose, arabinose, galactose, xylose, and formate were bought from Sigma-Aldrich (St. Louis, MO, USA). MWCNTs were obtained from CheapTubes.com (Brattleboro, VA, USA). Chloroplatinic acid ($H_2PtCl_6 \cdot 6H_2O$), peroxidase horseradish (HRP), 3,3',5,5'-tetramethylbenzidine (TMB) and superoxide dismutase (SOD) were purchased from Macklin (Shanghai, China). N-hydroxysuccinimide (NHS) and

View Article Online
DOI: 10.1039/D0NR04060F

1-ethyl-3-(3-dimethylaminopropyl) carbodiimide hydrochloride (EDC) were from J&K Scientific (Beijing, China). 1-Benzyl-1,4-dihydronicotinamide (BNAH) was from Bidepharm (Shanghai, China). All solutions were prepared with the deionized water purified with a Millipore-Q purification system (specific resistance > 18.0 MΩ cm). Formate dehydrogenase (FDH) and xylose dehydrogenase (XDH) were prepared according to previous methods.[62-63]

Published on 21 August 2020. Downloaded by University of Rochester on 8/25/2020 9:36:17 PM.

Apparatus.

Scanning electron microscopy (SEM) was carried out by using a SU8020 field emission SEM instrument (Hitachi, Japan) at an accelerating voltage of 3.0 kV with a EMAX x-stream^2 energy-dispersive X-ray analyzer (HORIBA, USA). Transmission electron microscope (TEM) was performed on a Tecnai G2 F30 field emission TEM instrument (FEI, Hillsboro, OR, USA) at an accelerating voltage of 80 kV. BET surface area was analyzed with an ASAP 2460 instrument (Micromeritics, USA). X-ray photoelectron spectroscopy (XPS) was conducted with an ESCALAB-250Xi system (Thermo Fisher Scientific, Waltham, MA, USA) using Al Kα as the X-ray source. Fourier transform infrared spectroscopy (FTIR) was carried out using a TENSOR II instrument (Bruker, Billerica, MA, USA). Time-dependent absorbance and UV-Vis absorbance spectra were recorded with a Cary 100 UV-Vis (Agilent Technologies, Santa Clara, CA, USA). A CHI 1000C potentiostat (CH Instruments, Chenhua, China) was used for electrochemical experiments. All potentials in this work were set versus Ag/AgCl.

Preparation of PtNPs@MWCNTs nanocomposite

The PtNPs@MWCNTs nanocomposite was synthesized by growing the PtNPs *in situ* on the surface of carboxylated MWCNTs. Briefly, 100 mg MWCNTs, 10 mL 19 mM H_2PtCl_6 and 10 mL 40 mM KOH were added into a three-necked flask and sonicated for 30 min. Then, 25 mL ethylene glycol as a reducing agent was added into the above-mentioned solution dropwisely under vigorous stirring for 2 h at 130 °C. The black suspension was treated by centrifugation and washed 3 times with acetone.

Nanoscale Accepted Manuscript

View Article Online
DOI: 10.1039/D0NR04060F

Finally, the product was oven-dried and stored at room temperature before use, with approximate 3.81% Pt in per milligram PtNPs@MWCNTs (Fig. S8).

Catalytic activity of the PtNPs@MWCNTs for NADH oxidation

The catalytic activity of the PtNPs@MWCNTs was measured in 0.2 M disodium hydrogen phosphate and 0.1 M citric acid buffer (pH 5) containing 0.2 mM NADH at 25 °C. The decrease in the absorbance at 340 nm after the addition of 0.4 mg mL^{-1} PtNPs@MWCNTs was measured. The change in absorbance response was given by $\Delta Abs=Abs_{0\ min}-Abs_{1\ min}$. The influences of temperatures (15-80 °C) and pHs (3.0-10.0) were investigated.

In a steady-state kinetic assay, the catalytic reaction of the PtNPs@MWCNTs was determined by varying the concentration of NADH from 0.05 mM-10 mM under the standard condition. The concentration of oxidized NADH was calculated using a molar absorption coefficient of 6.22 mM^{-1} cm^{-1}. The apparent steady-state reaction velocity was obtained by calculating the slope of initial absorbance change with time. Accordingly, Michaelis-Menten and Lineweaver-Burk plots were drawn.

Catalytic mechanism of the PtNPs@MWCNTs

The verification of reaction products was performed in the same buffer mentioned above at 25 °C. The specific steps are as follows: 5 μg mL^{-1} TMB and 0.2 mM H_2O_2 under a protective atmosphere of N_2 for 30 min were catalyzed by 1 μg mL^{-1} HRP as a control. 0.2 mM NADH was oxidized by 0.4 mg mL^{-1} PtNPs@MWCNTs nanozyme for 5 min and then the nanozyme was removed by centrifugation. After purging the supernatant with N_2 for 30 min, 1 μg mL^{-1} and 5 μg mL^{-1} TMB were added into the solution for UV-Vis absorbance spectra.

The effect of radical scavengers was evaluated by mixing 0.2 mM NADH and 0-0.1 mM NaN_3 or 0-100 U mL^{-1} SOD with 0.4 mg mL^{-1} nanozyme and detecting the time-dependent absorbance change at 340 nm for NADH. (NaN_3 was a well known $OH^{\bullet}$ and $^1O_2$ scavenger and SOD was a well known $O_2^{-\bullet}$ scavenger).

Published on 21 August 2020. Downloaded by University of Rochester on 8/25/2020 9:36:17 PM.

Nanoscale Accepted Manuscript

View Article Online
DOI: 10.1039/D0NR04060F

Bioactive NAD^+ regeneration and turnover number of the PtNPs@MWCNTs

Bioactive NAD^+ regeneration was measured as follows: 0.2 mM NADH was oxidized by 0.4 mg mL^{-1} PtNPs@MWCNTs nanozyme for 20 min until complete oxidization, and the nanozyme was removed by centrifugation. Then, 10 U FDH and 50 mM formate were added and the time-dependent absorbance change at 340 nm for NADH was monitored.

The total turnover number (TTN) of PtNPs@MWCNTs nanozyme was measured in the above-mentioned buffer containing 5 M formate, 10 U FDH, 0.5 mM NAD^+ and 0.4 mg mL^{-1} PtNPs@MWCNTs nanozyme. The TTN was calculated by the follow formula:

$$\mathrm{TTN} = \frac{c_{formate_{0\,h}} - c_{formate_{48\,h}}}{c_{NAD^+}}$$

Electrochemical performance of the PtNPs@MWCNTs

The electrochemical performance of the PtNPs@MWCNTs was measured in the blank buffer or buffer containing NADH, where bare GCE or GCEs with 10 μL 7 mg mL^{-1} MWCNTs or PtNPs@MWCNTs dropped were used as the working electrode, Pt wire was used as the counter electrode and Ag/AgCl was used as the reference electrode. Cyclic voltammetry (CV) was measured from -0.3 V to 0.7 V at a scan rate of 10 mV s^{-1}.

Evaluation of the PtNPs@MWCNTs for BNAH

The catalytic activity of the PtNPs@MWCNTs for BNAH was measured in the above-mentioned buffer containing 0.5 mM BNAH at 25 °C. The decrease in the absorbance at 340 nm after the addition of 0.4 mg mL^{-1} PtNPs@MWCNTs was measured. The change in absorbance response was given by $\Delta Abs = Abs_{0\ min} - Abs_{1\ min}$. The steady-state kinetic assay was determined by varying the concentration of NADH from 0-10 mM. The CV was obtained from -0.3 V to 0.7 V at a scan rate of 10 mV s^{-1}, by using a GCE with 10 μL 7 mg mL^{-1} nanozyme dropped as the working electrode in the buffer containing different concentrations of BNAH.

Published on 21 August 2020. Downloaded by University of Rochester on 8/25/2020 9:36:17 PM.

Nanoscale Accepted Manuscript

View Article Online
DOI: 10.1039/D0NR04060F

Published on 21 August 2020. Downloaded by University of Rochester on 8/25/2020 9:36:17 PM.

Fabrication of bioelectrodes and detection of xylose

Seventy mM EDC and 70 mM NHS were poured into 0.5 mL 2 mg mL^{-1} PtNPs@MWCNTs to activate the carboxyl groups for 1 h at 25 °C. After the incubation, 55 U XDH was mixed with PtNPs@MWCNTs at 4 °C overnight to form the XDH&PtNPs@MWCNTs complex. Next, the complex was centrifuged to remove excessive XDH and then re-dispersed in 1 mL ultrapure water with a final concentration of 40 U mL^{-1} XDH and 1 mg mL^{-1} PtNPs@MWCNTs. Finally, 2.5 μL XDH&PtNPs@MWCNTs complex was dropped on a GCE. The bioelectrode was designated as XDH&PtNPs@MWCNTs/GCE and stored at 4 °C under a dry condition when not in use. The homemade XDH was purified and examined by sodium dodecyl sulfate polyacrylamide gel electrophoresis (SDS-PAGE). FTIR was used to verify the effective construction of bioelectrodes. The electrochemical impedance spectroscopy (EIS) was performed at the open circuit potential over an AC frequency range of 100 kHz to 1 Hz, with a sinusoidal perturbation of 5 mV, in order to obtain the resistance of bioelectrodes.

The constructed XDH&PtNPs@MWCNTs/GCE bioelectrode was assayed in 5 mL 0.1 M PBS (pH 7.0) with 1 mM free NAD^+. The xylose or xylose-containing real sample added could be catalyzed by XDH and transformed into xylonolactone, where NAD^+ turned into NADH. The amperometric curve (i-t) was measured at the potential of 0.25 V with Pt wire as the counter electrode. The current response with or without xylose was recorded as i_{p0} or i_p. and their difference was given by $\Delta i_p = i_p - i_{p0}$.

Electronic Supplementary Information

The Supporting Information is available free of charge on the RSC Publications website.

Conflicts of interest

Z.Z., H.S., and C.M. claim the financial interest to the technique disclosed in this study and have applied two Chinese patents.

Nanoscale Accepted Manuscript

View Article Online
DOI: 10.1039/D0NR04060F

Published on 21 August 2020. Downloaded by University of Rochester on 8/25/2020 9:36:17 PM.

Acknowledgement

This work was supported by National Natural Science Foundation of China (21878324), Natural Science Foundation of Tianjin City (19JCYBJC24600) and the CAS Pioneer Hundred Talent Program (Type C, reference # 2016-081).

References

1 J. Wu, X. Wang, Q. Wang, Z. Lou, S. Li, Y. Zhu, L. Qin and H. Wei, *Chem. Soc. Rev.*, 2019, **48**, 1004-1076.

2 H. Wei and E. Wang, *Chem. Soc. Rev.*, 2013, **42**, 6060-6093.

3 D. W. Jiang, D. L. Ni, Z. T. Rosenkrans, P. Huang, X. Y. Yan and W. B. Cai, *Chem. Soc. Rev.*, 2019, **48**, 3683-3704.

4 Y. Y. Huang, J. S. Ren and X. G. Qu, *Chem. Rev.*, 2019, **119**, 4357-4412.

5 X. Wang, X. J. Gao, L. Qin, C. Wang, L. Song, Y.-N. Zhou, G. Zhu, W. Cao, S. Lin, L. Zhou, K. Wang, H. Zhang, Z. Jin, P. Wang, X. Gao and H. Wei, *Nat. Commun.*, 2019, **10**,704

6 L. Huang, J. Chen, L. Gan, J. Wang and S. Dong, *Science Advances*, 2019, **5**, eaav5490.

7 L. Z. Gao, J. Zhuang, L. Nie, J. B. Zhang, Y. Zhang, N. Gu, T. H. Wang, J. Feng, D. L. Yang, S. Perrett and X. Yan, *Nat. Nanotechnol.*, 2007, **2**, 577-583.

8 Y. Liu, H. H. Wu, Y. Chong, W. G. Wamer, Q. S. Xia, L. N. Cai, Z. H. Nie, P. P. Fu and J. J. Yin, *Acs*
Appl. Mater. Inter., 2015, **7**, 19709-19717.

9 C. J. Yu, T. H. Chen, J. Y. Jiang and W. L. Tseng, *Nanoscale*, 2014, **6**, 9618-9624.

10 B. Xu, H. Wang, W. Wang, L. Gao, S. Li, X. Pan, H. Wang, H. Yang, X. Meng, Q. Wu, L. Zheng, S.
Chen, X. Shi, K. Fan, X. Yan and H. Liu, *Angew. Chem. Int. Ed.*, 2019, **58**, 4911-4916.

11 W. S. Kong, X. X. Guo, M. Jing, F. L. Qu and L. M. Lu, *Biosens. Bioelectron.*, 2020, **150**, 111875.

12 M. N. Ivanova, E. D. Grayfer, E. E. Plotnikova, L. S. Kibis, G. Darabdhara, P. K. Boruah, M. R. Das
and V. E. Fedorov, *Acs Appl. Mater. Inter.*, 2019, **11**, 22102-22112.

13 J. Liu, L. Meng, Z. Fei, P. J. Dyson and L. Zhang, *Biosens. Bioelectron.*, 2018, **121**, 159-165.

14 H. Chen, Q. Qiu, S. Sharif, S. Ying, Y. Wang and Y. Ying, *Acs Appl. Mater. Inter.*, 2018, **10**, 24108-24115.

15 Y. Huang, M. Zhao, S. Han, Z. Lai, J. Yang, C. Tan, Q. Ma, Q. Lu, J. Chen, X. Zhang, Z. Zhang, B. Li, B. Chen, Y. Zong and H. Zhang, *Adv. Mater.*, 2017, **29**, 1700102.

16 A. J. Clark, E. L. Coury, A. M. Meilhac and H. R. Petty, *Nanotechnology*, 2016, **27**, 065101.

17 Q. Liu, Y. Yang, X. Lv, Y. Ding, Y. Zhang, J. Jing and C. Xu, *Sens. Actuat. B: Chem.*, 2017, **240**, 726-734.

18 W. Xu, L. Jiao, H. Yan, Y. Wu, L. Chen, W. Gu, D. Du, Y. Lin and C. Zhu, *Acs Appl. Mater. Inter.*, 2019, **11**, 22096-22101.

19 X. J. Wu, T. M. Chen, J. X. Wang and G. W. Yang, *J. Mater. Chem. B*, 2018, **6**, 105-111.

20 D. V. Vokhmyanina, K. D. Andreeva, M. A. Komkova, E. E. Karyakina and A. A. Karyakin,

Nanoscale Accepted Manuscript

View Article Online
DOI: 10.1039/D0NR04060F

Talanta,
2020, **208**, 120393.
21 F. Cao, L. Zhang, H. Wang, Y. You, Y. Wang, N. Gao, J. Ren and X. Qu, *Angew. Chem. Int. Ed.*, 2019, **58**, 16236-16242.
22 Z. Wang, Y. Zhang, E. Ju, Z. Liu, F. Cao, Z. Chen, J. Ren and X. Qu, *Nat. Comm.*, 2018, **9**, 3334.
23 A. Swaidan, P. Borthakur, P. K. Boruah, M. R. Das, A. Barras, S. Hamieh, J. Toufaily, T. Hamieh, S.
Szunerits and R. Boukherroub, *Sens. Actuat. B: Chem.*, 2019, **294**, 253-262.
24 G. Darabdhara, B. Sharma, M. R. Das, R. Boukherroub and S. Szunerits, *Sens. Actuat. B: Chem.*, 2017, **238**, 842-851.
25 Y. Ma, Z. Jin, B. Peng, J. Ding, N. Wang and M. Zhou, *J. Electrochem. Soc.*, 2015, **162**, H317-H320.
26 H. K. Song, S. H. Lee, K. Won, J. H. Park, J. K. Kim, H. Lee, S. J. Moon, D. K. Kim and C. B. Park, *Angew. Chem. Int. Ed.*, 2008, **47**, 1749-1752.
27 A. Radoi and D. Compagnone, *Bioelectrochemistry*, 2009, **76**, 126-134.
28 Y. Zhang, X. Bo, A. Nsabimana, C. Luhana, G. Wang, H. Wang, M. Li and L. Guo, *Biosens. Bioelectron.*, 2014, **53**, 250-256.
29 H. Mao, Y. Li, X. Liu, W. Zhang, C. Wang, S. S. Al-Deyab and M. El-Newehy, *J. Colloid Interface Sci.*, 2011, **356**, 757-762.
30 F. Gao, X. Guo, J. Yin, D. Zhao, M. Li and L. Wang, *RSC Adv.*, 2011, **1**, 1301.
31 M. Govindhan, M. Amiri and A. Chen, *Biosens. Bioelectron.*, 2015, **66**, 474-480.
32 P. P. Gai, C. E. Zhao, Y. Wang, E. S. Abdel-Halim, J. R. Zhang and J. J. Zhu, *Biosens. Bioelectron.*, 2014, **62**, 170-176.
33 W. Li, C. Bin, H. X. Zhang, Y. H. Sun, J. Wang, J. L. Zhang and Y. Fu, *Biosens. Bioelectron.*, 2015, **66**, 251-258.
34 S. B. He, H. H. Deng, A. L. Liu, G. W. Li, X. H. Lin, W. Chen and X. H. Xia, *Chemcatchem*, 2014, **6**, 1543-1548.
35 S. Y. Zhu, C. H. Lei, J. Sun, X. E. Zhao, X. Wang, X. L. Yan, W. Liu and H. Wang, *Sens. Actuat. B:*
Chem., 2019, **282**, 896-903.
36 Y. Yuan, R. Yuan, Y. Chai, Y. Zhuo, X. Ye, X. Gan and L. Bai, *Chem. Comm.*, 2012, **48**, 4621-4623.
37 J. Han, L. Jiang, F. Li, P. Wang, Q. Liu, Y. Dong, Y. Li and Q. Wei, *Biosens. Bioelectron.*, 2016, **77**,
1104-1111.
38 C. Wang, Y. Yang, R. Li, D. Wu, Y. Qin and Y. Kong, *Chem. Commun.*, 2020, **56**, 4003-4006.
39 S. Sahin, T. Wongnate, L. Chuaboon, P. Chaiyen and E. H. Yu, *Biosens. Bioelectron.*, 2018, **107**, 17-25.
40 S. Wang, J. Li, Y. Qiu, X. Zhuang, X. Wu and J. Jiang, *Appl. Surf. Sci.*, 2019, **487**, 766-772.
41 F. Luan, Y. Wang, S. Zhang, X. Zhuang, C. Tian, X. Fu and L. Chen, *Analyst*, 2020, **145**, 1943-1949.
42 D. Chen, X. Zhuang, J. Zhai, Y. Zheng, H. Lu and L. Chen, *Sens. Actuactors B Chem.*, 2018, **255**, 1500-1506.
43 Z. Wang, Y. Zhang, E. Ju, Z. Liu, F. Cao, Z. Chen, J. Ren and X. Qu, *Nat. Commun.*, 2018, **9**.

Published on 21 August 2020. Downloaded by University of Rochester on 8/25/2020 9:36:17 PM.

Nanoscale Accepted Manuscript

View Article Online
DOI: 10.1039/D0NR04060F

44 Y. Jiang, X. Zhao, J. Huang, J. Li, P. K. Upputuri, H. Sun, X. Han, M. Pramanik, Y. Miao, H. Duan, K. Pu and R. Zhang, *Nat. Commun.*, 2020, **11**, 1857-1857.

45 J. Liu, L. Meng, Z. Fei, P. J. Dyson and L. Zhang, *Biosens. Bioelectron.*, 2018, **121**, 159-165.

46 H.-H. Deng, X.-L. Lin, Y.-H. Liu, K.-L. Li, Q.-Q. Zhuang, H.-P. Peng, A.-L. Liu, X.-H. Xia and W. Chen, *Nanoscale*, 2017, **9**, 10292-10300.

47 Y. Lin, A. Zhao, Y. Tao, J. Ren and X. Qu, *J. Am. Chem. Soc.*, 2013, **135**, 4207-4210.

48 Lisa, Marx, Nicolás, Ríos‐Lombardía, Judith, F., Farnberger, Wolfgang, Kroutil and Ana, *Adv. Synth. Catal.*, 2018. **360**, 2157-2165.

49 E.-J. Kim, J.-E. Kim and Y.-H. P. J. Zhang, *Energ. Environ.Sci.*, 2018, **11**, 2064-2072.

50 H. Zhou, Z. Zhang, P. Yu, L. Su, T. Ohsaka and L. Mao, *Langmuir*, 2010, **26**, 6028-6032.

51 H. S. Toogood, T. Knaus and N. S. Scrutton, *Chemcatchem*, 2014, **6**, 951-954.

52 C. E. Paul, I. W. C. E. Arends and F. Hollmann, *ACS Catal.*, 2014, **4**, 788-797.

53 I. Zachos, C. Nowak and V. Sieber, *Curr. Opin. Chem. Biol.*, 2019, **49**, 59-66.

54 C. E. Paul and F. Hollmann, *Appl. Microbiol. Biotechnol.*, 2016, **100**, 4773-4778.

55 E. Campbell, M. Meredith, S. D. Minteer and S. Banta, *Chem. Commun.*, 2012, **48**, 1898-1900.

56 T. Knaus, C. E. Paul, C. W. Levy, S. de Vries, F. G. Mutti, F. Hollmann and N. S. Scrutton, *J. Am. Chem. Soc.*, 2016, **138**, 1033-1039.

57 R. Huang, H. Chen, D. M. Upp, J. C. Lewis and Y.-H. P. J. Zhang, *ACS Catal.*, 2019, **9**, 11709-11719.

58 C. Stephens, B. Christen, T. Fuchs, V. Sundaram, K. Watanabe and U. Jenal, *J. Bacteriol.*, 2007, **189**, 2181-2185.

59 K. Khaldi, S. Sam, A. Lounas, C. Yaddaden and N.-E. Gabouze, *Appl. Surf. Sci.*, 2017, **421**, 148-154.

60 S. Zhu, C. Lei, J. Sun, X.-E. Zhao, X. Wang, X. Yan, W. Liu and H. Wang, *Sens. Actuactors B Chem.*, 2019, **282**, 896-903.

61 Y. L. Yuan, R. Yuan, Y. Q. Chai, Y. Zhuo, X. Y. Ye, X. X. Gan and L. J. Bai, *Chem. Commun.*, 2012, **48**, 4621-4623.

62 H. Song, C. Ma, P. Liu, C. You, J. Lin and Z. Zhu, *Journal of CO2 Utilization*, 2019, **34**, 568-575.

63 L. Li, B. Liang, F. Li, J. Shi, M. Mascini, Q. Lang and A. Liu, *Biosens. Bioelectron.*, 2013, **42**, 156-162.

Published on 21 August 2020. Downloaded by University of Rochester on 8/25/2020 9:36:17 PM.

Nanoscale Accepted Manuscript

View Article Online
DOI: 10.1039/D0NR04060F

Published on 21 August 2020. Downloaded by University of Rochester on 8/25/2020 9:36:17 PM.

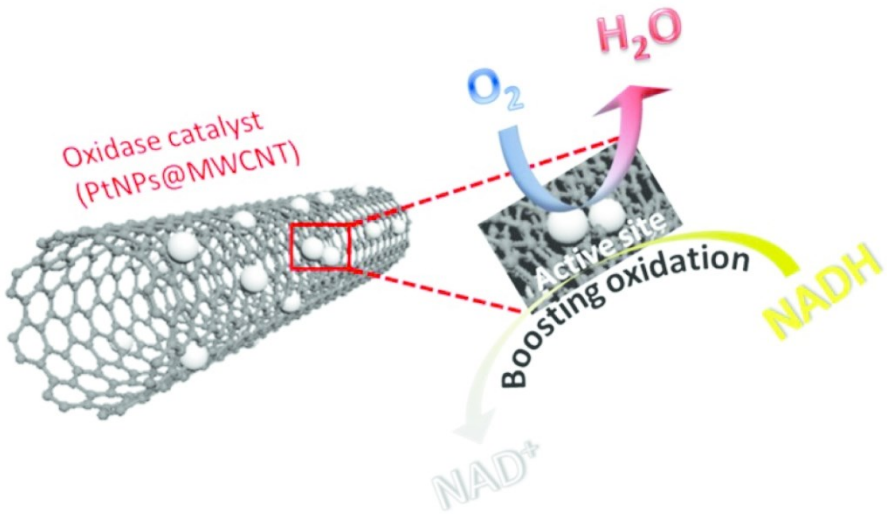

Nanoscale Accepted Manuscript